J Solid State Electrochem (2012) 16:9–16
DOI 10.1007/s10008-010-1270-y

ORIGINAL PAPER

Microstructure and electrochemical properties of porous $La_2NiO_{4+\delta}$ electrode screen-printed on $Ce_{0.8}Sm_{0.2}O_{1.9}$ electrolyte

Kai Zhao · Qing Xu · Duan-Ping Huang · Wen Chen · Min Chen · Bok-Hee Kim

Received: 26 September 2010 / Revised: 26 November 2010 / Accepted: 29 November 2010 / Published online: 16 December 2010

Abstract Superfine and uniform $La_2NiO_{4+\delta}$ powder was synthesized by a polyaminocarboxylate complex precursor method. $La_2NiO_{4+\delta}$ layers were screen-printed on dense $Ce_{0.8}Sm_{0.2}O_{1.9}$ electrolyte substrates and sintered at 900–1,100 °C. The microstructure and electrochemical properties of the resulting porous electrodes were investigated with respect to sintering temperature. The results indicate a significant effect of sintering temperature on the microstructure and electrode polarization. It was found that elevating sintering temperature was favorable to the charge transfer process whereas undesired for the oxygen surface exchange process due to an increase of the grain size. Sintering at 900 °C was determined to be preferred in terms of the polarization resistance of the electrode. The porous electrode sintered at the temperature showed a fine-grained microstructure (about 200 nm) and a relatively low polarization resistance of 0.28 Ω cm^2 at 800 °C. This work suggests that preparing the electrode from superfine starting powder is contributive to modifying the polarization properties.

K. Zhao · Q. Xu (✉) · D.-P. Huang · W. Chen
School of Materials Science and Engineering,
Wuhan University of Technology,
Wuhan 430070, People's Republic of China
e-mail: xuqing@whut.edu.cn

M. Chen · B.-H. Kim
Development of Hydrogen and Fuel Cell Engineering, Hydrogen and Fuel Cell Research Center, Chonbuk National University,
Jeonju 561756, South Korea

Present Address:
M. Chen
Department of Chemical and Materials Engineering,
University of Alberta,
Edmonton, AB T6G 2R3, Canada

Keywords $La_2NiO_{4+\delta}$ · Porous electrode · Microstructure · Polarization · Screen-printing

Introduction

Solid oxide fuel cells (SOFCs) are energy conversion devices with high efficiency and environmental advantages. There has been a continuous effort to reduce the operation temperature of SOFCs down to intermediate temperatures (600–800 °C) or less. As for the intermediate temperature SOFCs (IT-SOFCs), one of the major problems encountered is increased polarization loss from the cathodes at the reduced temperatures, leading to a performance degradation of the cells. Adopting electronic-ionic mixed conductors as the cathodes has been well recognized as a feasible solution to solve the problem due to extended electrochemical reaction region and promoted cathodic reaction kinetics at the intermediate temperatures. Extensive researches have been conducted to develop novel mixed-conducting cathode materials with desired overall properties. Recently, $Ln_2NiO_{4+\delta}$-based mixed conductors have drawn much attention as promising candidate materials for the cathode of IT-SOFCs because of their high oxygen diffusion and surface exchange coefficients at the intermediate temperatures together with moderate thermal expansion coefficients around 13.0×10^{-6} K^{-1} [1, 2].

The cathodic polarization of a SOFC device usually accounts for a dominant part of the whole cell polarization [3]. Therefore, electrocatalytic activity towards oxygen reduction is an important criterion to assess the application potential of a cathode material in SOFC devices. The electrochemical properties of $Ln_2NiO_{4+\delta}$-based mixed conductors have been extensively examined

in view of the IT-SOFC application [4–8]. Meanwhile, oxygen reduction reaction on the surfaces of $Ln_2NiO_{4+\delta}$-based cathodes has been investigated by the electrochemical impedance spectroscopy technique under various dc bias levels and/or oxygen partial pressures [9–15]. Moreover, the performances of $Ln_2NiO_{4+\delta}$-based cathodes in IT-SOFC devices have been evaluated [3, 7, 15]. Despite these previous works, there has been little research on the electrochemical properties of $Ln_2NiO_{4+\delta}$-based cathodes with respect to their microstructures. As has been well established, the electrochemical activity of a cathode working with an electrolyte is highly microstructure-dependent, related with the grain size, connection between the grains and porosity of the cathode as well as the adhesion of the cathode to the electrolyte [16, 17]. Such dependence thus warrants a research regarding the effect of microstructure on electrochemical properties for $Ln_2NiO_{4+\delta}$-based cathodes.

In continuation to our earlier research on synthesizing superfine $La_2NiO_{4+\delta}$ powder via a polyaminocarboxylate complex route [18], we prepared porous $La_2NiO_{4+\delta}$ electrodes on dense $Ce_{0.8}Sm_{0.2}O_{1.9}$ electrolyte substrates by a screen-printing technique. In this work, the polarization properties of the porous $La_2NiO_{4+\delta}$ electrodes were investigated in relation to their microstructures.

Experimental

$La_2NiO_{4+\delta}$ powder was synthesized by a polyaminocarboxylate complex precursor method. Reagent grade $La(OH)_3$, $NiCO_3{\cdot}2Ni(OH)_2{\cdot}4H_2O$, and diethylenetriaminepentaacetic acid (H_5DTPA) were used as starting materials. The starting materials were dissolved into deionized water and stirred to form a transparent aqueous solution. The mole ratio of H_5DTPA to the total cation content was 1.7:3.0. The solution was heated to yield a solid polyaminocarboxylate complex. The solid complex precursor was pulverized and calcined at 900 °C for 2 h in air. X-ray diffraction (XRD) analysis identified a pure K_2NiF_4 phase for the calcined powder. The details of the synthesis process have been described elsewhere [18]. $Ce_{0.8}Sm_{0.2}O_{1.9}$ powder was synthesized by a urea-combustion method. Reagent grade $Ce(NO_3)_3{\cdot}6H_2O$, $Sm(NO_3)_3{\cdot}6H_2O$, and urea ($CO(NH_2)_2$) were used as starting materials. The starting materials were dissolved into deionized water to form a solution and then heated on a hot plate until auto-igniting combustion occurred. XRD analysis certified that the combusted powder had a pure cubic fluorite phase. After wet ball-milling, the combusted powder was compacted into pellets and sintered at 1,250 °C for 4 h in air. The Archimedes measurement indicated that the ceramic pellets attained about 96% of the theoretical density. The synthesis and preparation of $Ce_{0.8}Sm_{0.2}O_{1.9}$ ceramics have been previously reported [19].

$La_2NiO_{4+\delta}/Ce_{0.8}Sm_{0.2}O_{1.9}/La_2NiO_{4+\delta}$ symmetrical cells were fabricated using a screen-printing technique. $Ce_{0.8}Sm_{0.2}O_{1.9}$ ceramic pellets were polished to a thickness of 0.14 cm. $La_2NiO_{4+\delta}$ powder was mixed with organic solution to form a slurry-type ink. The organic solution was composed of ethyl cellulose ethoce (9 wt.%), dibutyl phthalate (10 wt.%), butyl alcohol (10 wt.%), silane coupling agent KH-570 (4 wt.%), and terpineol (67 wt. %). The weight fraction of $La_2NiO_{4+\delta}$ powder in the ink was 70%. The ink was screen-printed on both surfaces of the ceramic pellets and sintered at 900–1,100 °C for 2 h in air. The electrode area was about 0.79 cm^2. Platinum meshes were placed on the $La_2NiO_{4+\delta}$ electrodes as current collector. The electrochemical impedance spectra of the cells were measured at a CHI660C electrochemical workstation between 600 and 800 °C in air. The measurement was performed under zero dc bias in the frequency range of 0.01 Hz–100 kHz. The amplitude of input sinuous signals was 5 mV. The measured data were analyzed by the Zview 3.1a software.

The morphology of $La_2NiO_{4+\delta}$ powder was observed at a Hitachi S-4700 field emission scanning electron microscope (FESEM). The specific surface area of the powder was measured by the Brunauer–Emmett–Teller (BET) method at a Micromeritics Gemini 2380 surface area analyzer using liquid nitrogen adsorbent. The microstructures of the cells were investigated by a JEOL JSM-5610LV scanning electron microscope (SEM). The distributions of grain size and pore diameter of the electrodes were determined form image analysis using the Image Plus software. The porosity of the electrodes was estimated based on counting black and gray pixels of SEM micrographs, which refer to pores and grains, respectively [20].

Results and discussion

Figure 1 shows the FESEM micrograph of $La_2NiO_{4+\delta}$ powder. The powder consisted of uniform particles of around 100 nm. The BET analysis indicated that the powder had a specific surface area of 5.6 $m^2\ g^{-1}$. The average particle size of the powder was determined to be 95 nm based on the specific surface area, which is generally consistent with the FESEM observation.

Figure 2 shows the SEM micrographs of the cells sintered at different temperatures. The cross-section views (Fig. 2a, c, and e) indicated that the $La_2NiO_{4+\delta}$ electrodes were porous and had a good adhesion to the electrolyte supports. Moreover, the thicknesses of the electrodes steadily decreased from 36 to 17 μm with the elevation

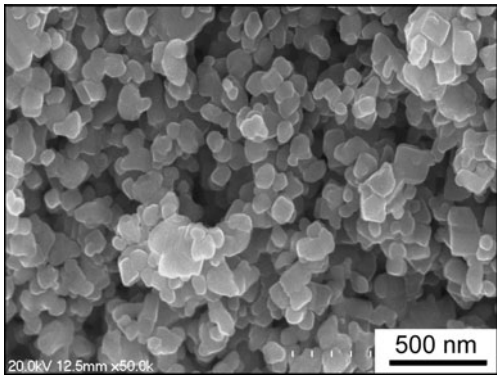

Fig. 1 FESEM micrograph of $La_2NiO_{4+\delta}$ powder

of sintering temperature from 900 to 1,100 °C, which can be attributed to the shrinkage of the electrodes during sintering. The surface views (Fig. 2b, d, and f) illustrated well-connected grains and uniformly distributed micropores of the electrodes. Figure 3 shows the distributions of the grain size and pore diameter of the electrode sintered at 900 °C. The distributions generally agree with a Gaussian fitting. Similar results were obtained for the electrodes sintered at other temperatures. Figure 4 shows the average grain sizes and porosities of the $La_2NiO_{4+\delta}$ electrodes sintered at different temperatures. The porosities of the electrodes slightly varied in the range of 17–20%, while the average grain sizes monotonically increased from about 200 to about 700 nm with the elevation of sintering temperature.

Figure 5 shows the impedance spectra measured at different temperatures for the cells sintered at 900 and 1,100 °C, respectively. The cells sintered at other temperatures presented analogous spectra. Inductive impedance response was detected for each impedance spectrum, appearing as a high frequency tail below the real axis. The inductive responses were subtracted from the spectra

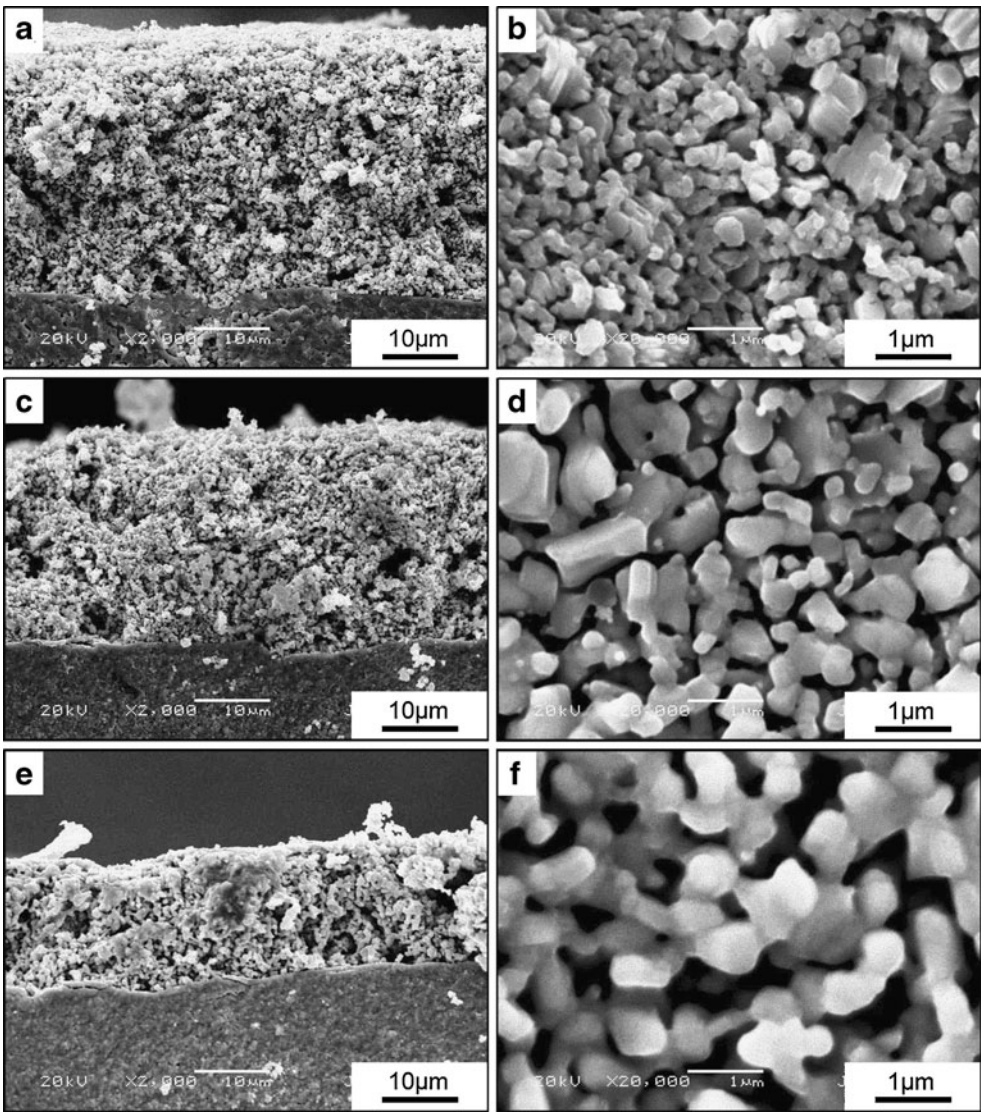

Fig. 2 SEM micrographs of $La_2NiO_{4+\delta}$ electrodes sintered at different temperatures: **a** cross-section view (900 °C), **b** surface view (900 °C), **c** cross-section view (1,000 °C), **d** surface view (1,000 °C), **e** cross-section view (1,100 °C), and **f** surface view (1,100 °C)

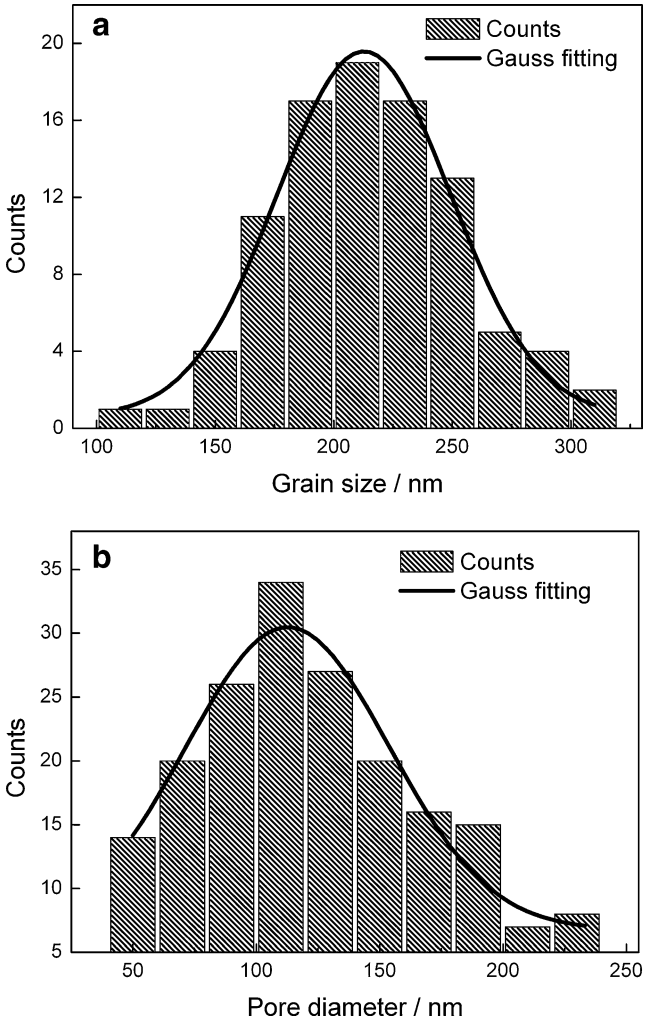

Fig. 3 Distributions of **a** grain size and **b** pore diameter of $La_2NiO_{4+\delta}$ electrode sintered at 900 °C

because, as well known, they were caused by the measuring device and connecting wires. The spectra are obviously asymmetrical in shape, implying contributions from more than one electrode process. The impedance spectra were fitted according to a $R_{el}(R_1Q_1)(R_2Q_2)(R_3Q_3)$ equivalent circuit model, as shown in Fig. 6. The R_{el} refers to the ohmic resistance of the cell and the (RQ) components correspond to involved electrode processes. The R is a resistance and the Q is a constant phase element (CPE). The impedance Z_Q and equivalent capacitance C of a constant phase element Q can be calculated according to the following equations [21]:

$$Z_Q = \frac{1}{Q(i\cdot\omega)^n} \tag{1}$$

$$C = \frac{(R\cdot Q)^{1/n}}{R} \tag{2}$$

Where the ω is the angular frequency and n is an exponent. The relaxation frequency f of an electrode process corresponding to a specific (RQ) component can be calculated by the following equation [21]:

$$f = \frac{(R\cdot Q)^{-1/n}}{2\pi} \tag{3}$$

From Fig. 5, it can be seen that the fitting results agree well with the experimental data. For the cells sintered at other temperatures, the spectrum fitting also attained a reasonable agreement with measured data.

The spectrum fitting results of the cell sintered at 900 °C are listed in Table 1. The parameters were normalized with the configuration and geometrical factors of the cell. The equivalent capacitances and relaxation frequencies can be applied as characteristic parameters to identify the processes [11, 21]. The electrode processes corresponding to the (R_1Q_1) and (R_2Q_2) components showed the equivalent capacitances of 10^{-5}–10^{-4} and 10^{-4}–10^{-3} F cm^{-2} together with the relaxation frequencies of 10^2–10^4 and 10–10^3 Hz, respectively. Accordingly, the former process can be attributed to the charge transfer at the interface between the electrode and electrolyte while the latter one can be ascribed to the oxygen exchange on the surface of the electrode [13, 22]. The electrode process corresponding to the component (R_3Q_3) showed an equivalent capacitance of 10^{-1} F cm^{-2} and a relaxation frequency of about 10 Hz. In order of magnitude, the equivalent capacitance is too large to be related to an interfacial electrochemical reaction [23]. This process is assigned to the diffusion of oxygen gas to the surface of the electrode, which is consistent with literature results [11, 13].

The polarization resistances of the charge transfer process (R_1) and the oxygen surface exchange process

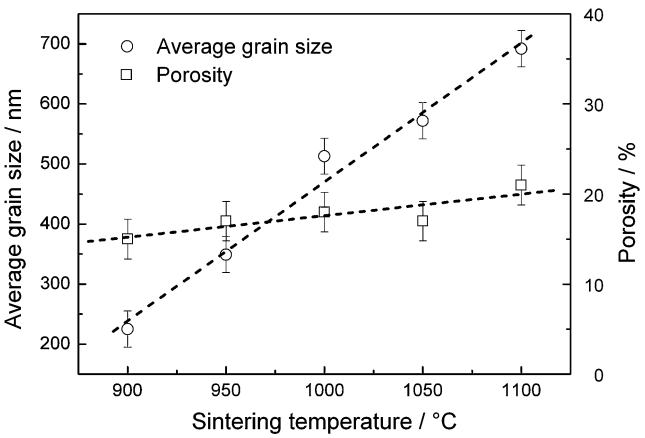

Fig. 4 Average grain sizes and porosities of $La_2NiO_{4+\delta}$ electrodes sintered at different temperatures

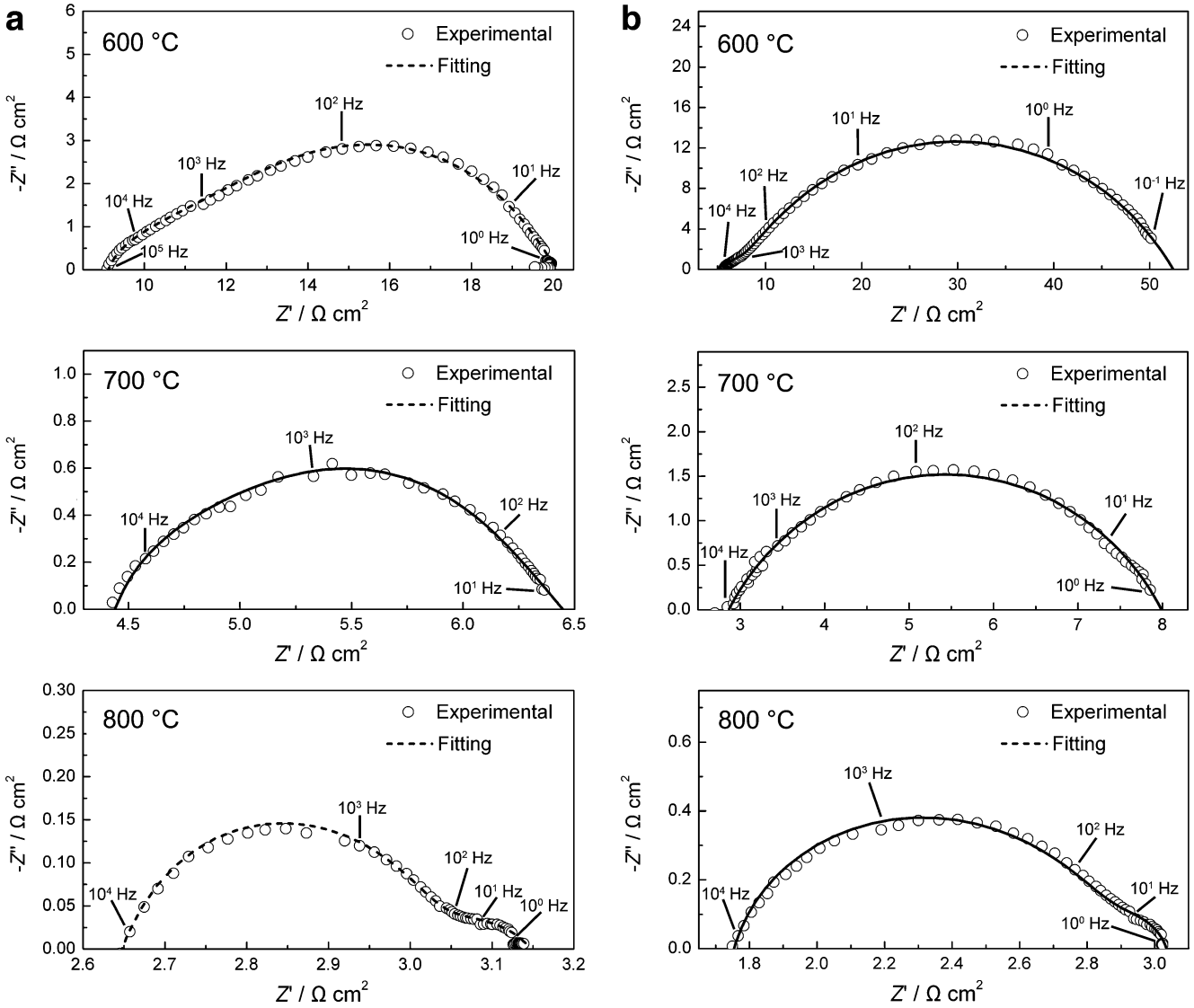

Fig. 5 Impedance spectra measured at different temperatures (600, 700, and 800 °C) for the cells sintered at **a** 900 °C and **b** 1,100 °C

(R_2) decreased with increasing measuring temperature. The impedance response of the charge transfer process disappeared at 800 °C. Meanwhile, an additional impedance response associated with the oxygen gas-phase diffusion process appeared. Similar phenomenon has been reported for $PrBaCo_2O_{5+\delta}$ cathode material [21]. This spectrum evolution indicates the influence of the oxygen-ion transport properties of $La_2NiO_{4+\delta}$ on the electrode reaction. It has been reported that the oxygen diffusion and surface exchange coefficients of $La_2NiO_{4+\delta}$ increase with higher temperatures [14]. Therefore, increasing measuring temperature favors the charge transfer and oxygen surface exchange processes, leading to a decline of the R_1 and R_2. The disappearance of the impedance response of the charge transfer process at 800 °C can be ascribed to a facilitated oxygen-ion transport at the elevated temperature. By comparison, the oxygen gas-phase diffusion process is somewhat thermally insensitive [24]. As a result, the non-chemical process can not match in kinetics with the facilitated electrochemical processes at elevated temperatures, which generates concentration polarization. The appearance of the additional impedance response at 800 °C can be attributed to this dynamic reason.

Similar spectrum fitting results were obtained for the cells sintered at other temperatures. The polarization resistances of the electrodes sintered at different temperatures are summarized in Table 2. At an identical measuring temperature, the R_1 values tended to reduce with increasing sintering temperature, whereas the R_2 values showed an inverse trend. The R_3 values of the cells sintered at different temperatures are roughly similar

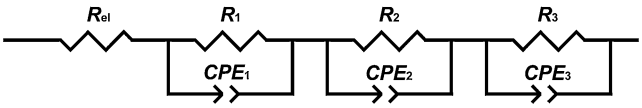

Fig. 6 Equivalent circuit model of impedance spectrum fitting

in magnitude, acting as a minor contribution to the total electrode polarization. In general, the polarization resistances of the overall electrode reaction (R_p) became larger with increasing sintering temperature. Figure 7 shows the Arrhenius plots of the R_p for the electrodes sintered at different temperatures. The plots displayed a basically linear relation. The activation energies (E_a) of the overall electrode reaction were determined from a linear fitting of the plots. The electrodes sintered at different temperatures showed the activation energies of about 1.2–1.4 eV, as shown in the inserted table in Fig. 7. These values are consistent with the typical results of surface oxygen reduction reaction determined from various mixed-conducting electrodes [4, 13, 25].

It can be noticed that the polarization resistance of the electrode is significantly dependent on its sintering temperature. This dependence can be qualitatively interpreted in relation to the microstructure evolution of the electrodes. On one hand, increasing sintering temperature can result in a tighter adhesion of the electrode to the electrolyte support, which benefits the charge transfer process. The decrease of the R_1 with increasing sintering temperature can be viewed as an evidence of the interface effect. On the other hand, the grain size of the electrode became obviously larger with increasing sintering temperature (Fig. 4). This case reduced the specific surface area, i.e., electrocatalytically active region, of the porous electrode, which is unfavorable to the surface oxygen exchange process. The increase of the R_2 with increasing sintering temperature can be ascribed to the grain size effect. Considering the minor contribution of the oxygen gas-phase diffusion process, the variation of the total electrode polarization with sintering temperature appears to rely on the competition of the two inverse effects.

At measuring temperature of 800 °C, the electrode sintered at 900 °C exhibited the lowest R_p of 0.28 Ωcm^2 among the investigated electrodes. This polarization resistance is competitive to the literature results (1.00 and 0.41 Ωcm^2) obtained at the same measuring temperature for $La_2NiO_{4+\delta}$ electrodes printed on $Ce_{0.8}Sm_{0.2}O_{1.9}$ and 2 mol % Co-doped $Ce_{0.8}Sm_{0.2}O_{1.9}$ supports, respectively [7]. Compared with the electrodes of the previous work (average grain size, ~500 nm), the electrode of the present work had finer grains (around 200 nm; Fig. 4). The low polarization resistance of the electrode in the present work can be related to its fine-grained microstructure. The fine-grained microstructure is regarded to be associated with the

Table 1 Results of impedance spectrum fitting for the cell sintered at 900 °C

Measuring temperature (°C)	$R_{el}\Omega$ cm^2	$R_1\Omega$ cm^2	CPE_1-$T\Omega$ cm^2 s^{-n}	CPE_1-P	C_1 F cm^{-2}	f_1Hz	$R_2\Omega$ cm^2	CPE_2-$T\Omega$ cm^2 s^{-n}	CPE_2-P	C_2F cm^{-2}	f_2Hz	$R_3\Omega$ cm^2	CPE_3-$T\Omega$ cm^2 s^{-n}	CPE_3-P	C_3 F cm^{-2}	f_3 Hz	$R_p\Omega$ cm^2
600	8.61	2.88	8.25×10^{-3}	0.45	8.93×10^{-5}	619	2.89	3.00×10^{-3}	0.80	9.12×10^{-4}	60	–	–	–	–	–	5.77
650	5.69	1.09	1.21×10^{-2}	0.45	6.47×10^{-5}	2,268	1.37	2.98×10^{-3}	0.76	5.10×10^{-4}	227	–	–	–	–	–	2.46
700	4.17	0.87	9.27×10^{-3}	0.53	1.26×10^{-4}	1,455	0.27	1.83×10^{-3}	0.94	1.11×10^{-3}	532	–	–	–	–	–	1.14
750	3.51	0.06	1.53×10^{-4}	1.00	1.53×10^{-4}	16,395	0.53	2.83×10^{-3}	0.74	2.70×10^{-4}	1,120	–	–	–	–	–	0.59
800	2.58	–	–	–	–	–	0.22	2.19×10^{-3}	0.80	3.23×10^{-4}	2,208	0.06	1.55×10^{-0}	0.54	2.14×10^{-1}	12	0.28

Table 2 Polarization resistances of $La_2NiO_{4+\delta}$ electrodes sintered at different temperatures

Sintering temperature (°C)	Measuring temperature (°C)	$R_1\,\Omega\ cm^2$	$R_2\,\Omega\ cm^2$	$R_3\,\Omega\ cm^2$	$R_p\,\Omega\ cm^2$
900	600	2.88	2.89	–	5.77
	650	1.09	1.37	–	2.46
	700	0.87	0.27	–	1.14
	750	0.06	0.53	–	0.59
	800	–	0.22	0.06	0.28
950	600	3.34	13.27	–	16.61
	650	3.04	3.66	–	6.70
	700	0.32	2.14	–	2.46
	750	–	1.02	–	1.02
	800	–	0.38	0.02	0.40
1,000	600	1.66	9.97	–	11.63
	650	0.80	4.39	–	5.19
	700	0.07	2.06	–	2.13
	750	–	1.12	–	1.12
	800	–	0.54	0.03	0.57
1,050	600	1.19	18.97	–	20.16
	650	1.04	7.16	–	8.20
	700	0.28	3.19	–	3.47
	750	0.09	1.56	–	1.65
	800	–	0.76	0.03	0.79
1,100	600	0.88	22.52	–	23.40
	650	0.38	6.95	–	7.33
	700	–	2.71	–	2.71
	750	–	1.26	0.08	1.34
	800	–	0.63	0.06	0.69

superfine morphology of the starting powder. Thus, preparing the electrode from superfine starting powder appears to be contributive to the modification of the polarization properties.

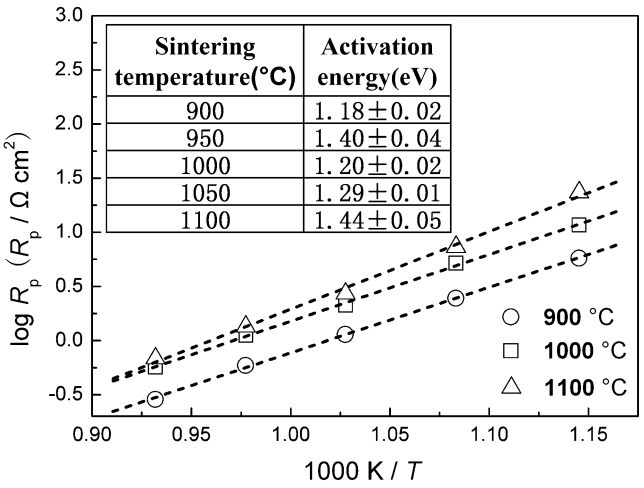

Fig. 7 Arrhenius plots of the overall polarization resistance (R_p) for $La_2NiO_{4+\delta}$ electrodes sintered at different temperatures

Conclusions

Superfine and uniform $La_2NiO_{4+\delta}$ powder was synthesized by a polyaminocarboxylate precursor method. $La_2NiO_{4+\delta}$ layers were screen-printed onto $Ce_{0.8}Sm_{0.2}O_{1.9}$ electrolyte substrates and sintered at 900–1,100 °C. The microstructure and polarization properties of the resulting porous electrodes have been investigated with respect to sintering temperature. The results demonstrate a significant role of sintering temperature on the microstructure and electrode polarization. It was detected that increasing sintering temperature was beneficial to the charge transfer process whereas unfavorable to the oxygen surface exchange process due to an increase of the grain size. The preferred sintering temperature of the electrode was determined to be 900 °C. The porous electrode sintered at the temperature showed a fine-grained microstructure (about 200 nm) and a relatively low polarization resistance of 0.28 Ω cm^2 at 800 °C. Producing the electrode from superfine starting powder is suggested to be advantageous to modifying the electrode properties.

Acknowledgments This work was supported by the Natural Science Foundation of China (50572079 and A3 Foresight Program-50821140308), Ministry of Education (200804971002), Wuhan Science and Technology Bureau (200851430485), and the Fundamental Research Funds for the Central Universities (2010-ZY-CL-060). The authors are grateful to the International Collaborative Research Program of Jeonbuk National University (2009) for supporting the research.

References

1. Kharton VV, Viskup AP, Naumovich EN, Marques FMB (1999) J Mater Chem 9(10):2623–2629
2. Skinner SJ, Kilner JA (2000) Solid State Ionics 135(1–4):709–712
3. Lalanne C, Mauvy F, Siebert E, Fontaine ML, Bassat JM, Ansart F, Stevens P, Grenier JC (2007) J Eur Ceram Soc 27(13–15):4195–4198
4. Amow G, Davidson IJ, Skinner SJ (2006) Solid State Ionics 177 (13–14):1205–1210
5. Mauvy F, Lalanne C, Fourcade S, Bassat JM, Grenier JC (2007) J Eur Ceram Soc 27(13–15):3731–3734
6. Aguadero A, Escudero MJ, Perez M, Alonso JA, Daza L (2007) J Fuel Cell Sci Technol 4(3):294–298
7. Pérez-Coll D, Aguadero A, Escudero MJ, Núñez P, Daza L (2008) J Power Sources 178(1):151–162
8. Kammer K (2009) Ionics 15(3):325–328
9. Kharton VV, Tsipis EV, Yaremchenko AA, Frade JR (2004) Solid State Ionics 166(3–4):327–337
10. Mauvy F, Lalanne C, Bassat JM, Grenier JC, Zhao H, Dordor P, Stevens P (2005) J Eur Ceram Soc 25(12):2669–2672
11. Mauvy F, Lalanne C, Bassat J-M, Grenier J-C, Zhao H, Huo L, Stevens P (2006) J Electrochem Soc 153(8):A1547–A1553
12. Li Q, Fan Y, Zhao H, Sun L-P, Huo L-H (2007) J Power Sources 167(1):64–68
13. Escudero MJ, Aguadero A, Alonso JA, Daza L (2007) J Electroanal Chem 611(1–2):107–116
14. Zhao H, Mauvy F, Lalanne C, Bassat JM, Fourcade S, Grenier JC (2008) Solid State Ionics 179(35–36):2000–2005
15. Pérez-Coll D, Aguadero A, Escudero MJ, Daza L (2009) J Power Sources 192(1):2–13
16. Lin Y, Barnett SA (2008) Solid State Ionics 179(11–12):420–427
17. Qiang F, Sun K, Zhang N, Le S, Zhu X, Piao J (2009) J Solid State Electrochem 13(3):455–467
18. Huang D-p, Xu Q, Zhang F, Chen W, Liu H-x, Zhou J (2006) Mater Lett 60(15):1892–1895
19. Chen M, Kim BH, Xu Q, Ahn BK, Kang WJ, Huang Dp (2009) Ceram Int 35(4):1335–1343
20. Choy KL, Charojrochkul S, Steele BCH (1997) Solid State Ionics 96(1–2):49–54
21. Chen D, Ran R, Zhang K, Wang J, Shao Z (2009) J Power Sources 188(1):96–105
22. Baumann FS, Fleig J, Habermeier H-U, Maier J (2006) Solid State Ionics 177(11–12):1071–1081
23. Adler SB, Lane JA, Steele BCH (1996) J Electrochem Soc 143 (11):3554–3564
24. Hart NT, Brandon NP, Day MJ, Lapeña-Rey N (2002) J Power Sources 106(1–2):42–50
25. Dusastre V, Kilner JA (1999) Solid State Ionics 126(1–2):163–174